ISSN 1590-8844
International Journal of Mechanics and Control, Vol. 25, No. 01, 2024
https://doi.org/10.69076/jomac.2024.0013

3D ANALYSIS OF THE MECHANICAL BEHAVIOUR FOR MATERIAL PROPERTIES BY USING TERAHERTZ IMAGING

Ilo Bodi*, Erald Piperi**, Morena Osmani***, Pascal Doumalin****, Jean – Christophe Dupre*****

* Department of Production and Management, Polytechnic University of Tirana
** Department of Production and Management, Polytechnic University of Tirana
*** Polytechnic University of Tirana
**** Institut Pprime, UPR CNRS 3346, Université de Poitiers
***** Institut Pprime, UPR CNRS 3346, Université de Poitiers

ABSTRACT

This paper shows how to comprehensively characterize the mechanical properties of diverse materials and structures using terahertz imaging. The investigation aims to explore and develop the potential of terahertz imaging by using digital image correlation (DIC) in the detailed characterization of mechanical behaviour. Terahertz waves, situated in the frequency range between microwaves and infrared (0.1 to 10 THz), possess distinctive properties that provide a significant advantage for penetrating various materials and structures without causing damage or ionization. Unique models were created, by using them as direct samples for the experiments. The development also included the creation of a loading post capable of applying forces in three directions compression, traction, and flexion providing a comprehensive approach to the material testing. The techniques of image analysis and processing, specifically in the context of 2D samples are used to obtain the material structures for further analysis. This was done through a series of tests conducted on different materials, such as glass fiber composites, non-composite CHC glass fiber, and a white structure featuring multiple holes. Terahertz imaging played a pivotal role in capturing and analysing the mechanical characteristics of these materials, thereby contributing valuable insights to the broader understanding of their behaviour.

Keywords: Terahertz imaging, Digital Image Correlation, Material structure, Material behaviour, 3D analysis,

1 INTRODUCTION

The inaugural terahertz (THz) images, captured in 1976 by T. S. Hartwick and colleagues, marked a groundbreaking achievement [1]. Employing an optically pumped molecular THz laser, they pioneered the exploration of terahertz frequencies. Subsequently, B. Hu and M. Nuss made a seminal contribution in 1995 [2], unveiling the principles of optoelectronic THz imaging through the utilization of femtosecond laser-based sources. This accomplishment ignited a wave of enthusiasm, leading to a surge in related activities.

Contact author: Ilo Bodi[1],

[1]Polytechnic University of Tirana, “Mother Theresa” Square, No.4, Tirana, Albania, AL 1001.
E-mail: ibodi@fim.edu.al

Over the past two decades, the domain of THz imaging has witnessed remarkable advancements, encompassing both fundamental research and diverse practical applications in different fields, also in industrial applications [3] [4] [5]. This progression underscores the dynamic nature of THz imaging science and technology.

The term "terahertz" frequencies, denoted as THz (where 1 THz equals 10^12 Hz), spans from 100 GHz to around 30 THz (Fig 1). This domain is characterized by wavelengths ranging approximately from 0.01 mm to 3 mm. Traditionally recognized as the far infrared region, it is also referred to in contemporary contexts as T-ray. Positioned within the electromagnetic spectrum, it resides between the infrared spectrum (of optics) and microwaves (associated with radioelectricity).

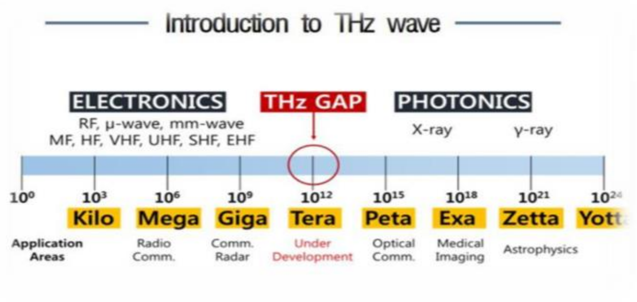

Figure 1 Terahertz frequencies [6].

Notably, THz imaging continues to serve as a fertile ground for innovative ideas, facilitating the convergence of disparate technologies and catalyzing their transformation into novel applications. This ongoing evolution positions THz imaging as an exciting and promising field, continually generating new insights and possibilities.

Being a new and exploratory study, that has not been used before for measuring mechanical quantities, it is necessary to collect various analytical and experimental data based on various previously performed experiments such as mechanical measurements through X-ray tomography. The experimental study of the mechanical behavior of materials and structures has been done using measurements of displacement fields, deformations, or stresses on the surface but also by volume measurements with X-ray tomography or optical tomography in the visible, which is why they are limited to low-density materials. This allows us to study whether such measurements are possible through terahertz waves, as they can be a complement to X-rays, in addition to other advantages they have over X-rays. These previously performed experiments will enable us to determine the actual possibilities of this method.

The work done in this study encompasses three primary objectives. First, extensive bibliographic research was made to unveil the intricacies of terahertz waves, their sources, underlying principles, and diverse applications, particularly within the field of mechanical engineering. Second, the focus shifts to the design of a storage and loading system integrated into the THz imaging acquisition system. Third, direct application with different materials preselected to conduct feasibility tests for mechanical measurements. This process includes sample selection, displacement measurement assessments (utilizing tracking markers and image correlation), as well as a comprehensive analysis of images, and the evolution of measurement performance. To successfully navigate these tasks, a combination of technological expertise, proficiency in mechanical engineering, and the application of mechanical tests and optical methods is indispensable.

2 MATERIALS AND METHODS

2.1 DESIGN OF THE LOADING SYSTEM

The characteristics of materials play a pivotal role in the manufacturing of diverse products, particularly in industrial settings. Consequently, a comprehensive exploration of the mechanical properties of materials is essential for understanding their response to stress, extent of deformation, and the strain they can withstand to mitigate potential damage. The primary objective of this project is to unveil the untapped potential of THz waves in the mechanical characterization of materials. This will be actualized through a systematic process involving compression, tension, and load application. The loading device will be mounted on the device for receiving images through THz waves, so we must take based on the dimensions and space that this element offers for design. The assembly of the pass within the Terahertz system will be done through aluminum profiles, as shown in Fig. 2.

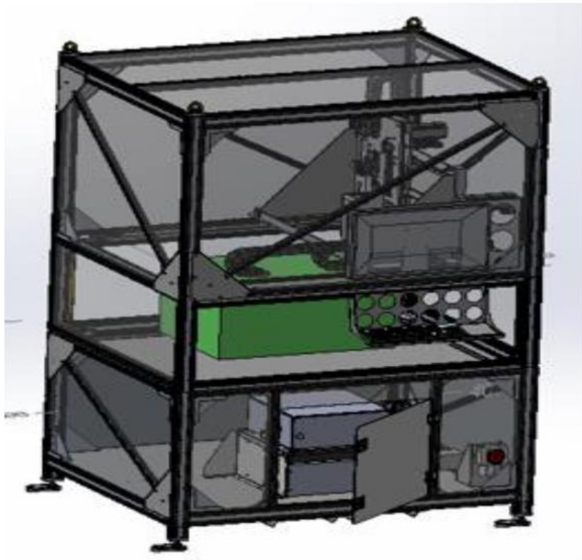

Figure 2 Terahertz setup optical coherent tomography device.

The measurement area has these dimensions: 800mm x 600mm x 400mm. The design concerns the development of a loading setup for an Optical coherent Tomography device
The system is equipped with a monitor through which the commands are given. Inside the system, there is a mobile camera through which images are taken. Its direction is from top to bottom. This can be said to have conditioned the design of the loading process after loading the material will be done in the up–down direction. However, this device will be attached to a movable translation stage in two directions (X-axis and Y-axis), so that capturing the images is easier.

The working principle is simple, the force required to compress the material/structure is generated by the motor (Fig. 3) and transmitted to the sample by an anvil designed for use with one of the bases of bent installations. This need arose due to the installation of the device within the THz system and during the material loading process it is not possible to do it mechanically. Through the motor, the "sliding"/movement of the structure will be enabled, which will load the material. Inside this chain is also the load, which measures the applied load. Through a guide system, the force is applied perpendicular to the surface of the sample.

ISSN 1590-8844
International Journal of Mechanics and Control, Vol. 25, No. 01, 2024

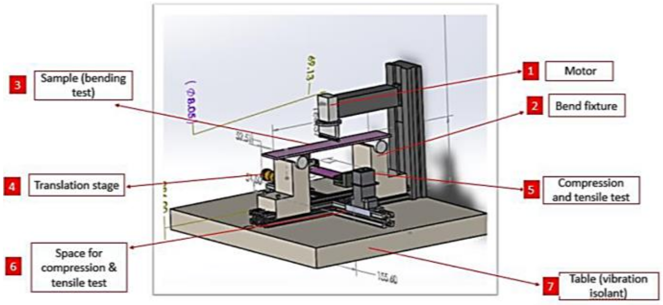

Figure 3 Terahertz device design and configuration.

The device consists of several other elements such as: 3-point bending test, with a motorized test stand, the base of the bending device contains blocks movable in both directions to be suitable for the size and type of the sample during bending with 3 points. In the same process, the bend fixture for compression and tension was built, which is adjusted through a translation stage with a selected accuracy of 10 µm. The base of the device will be a vibration isolator, to prevent movements that may affect the reception of low-quality images as shown in Figure 4.

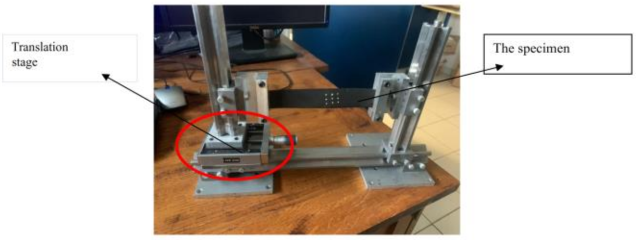

Figure 4 Loading machine production.

2.2 DIGITAL IMAGE CORRELATION

Digital Image Correlation (DIC) stands out as a cutting-edge measurement technique that leverages images captured by cameras to meticulously monitor and document the surface motion of a solid undergoing deformation. Over recent years, optical measurement techniques, particularly those embracing full-field and non-contact approaches, have demonstrated remarkable efficacy in capturing displacement and strain fields. Digital Image Correlation (DIC), in particular, has proven its adaptability and widespread utility in precisely measuring both 2D and 3D surfaces [7]. In the realm of experimental solid mechanics, the accurate assessment of strain and displacement in materials subjected to mechanical loads is a pivotal undertaking. In this context, DIC emerges as a valuable tool, offering intricate insights into the intricate dynamics of material behaviour during mechanical loading scenarios.
Access to a large amount of information is provided through CCD cameras. Each sensor pixel provides information encoded in several bits determined by the sensor's sensitivity (typically 8, 12 and 16 bits). This information corresponds to the luminous flux received at this pixel.

Each raw image is stored in the form of a 2D matrix, each box of which has a value called a gray level. These matrices are the input data of image correlation [8].
In this study the experimental measurements were obtained by DIC (Digital Image Correlation) for field displacement measurements and mark tracking method. The DIC process consist in calculating displacements on specific points defined by a virtual grid on a subset surrounding the considered point in both states.
The comparison of the two images is based on the hypothesis of optical flow conservation during loading: f(x)=g(x) which represent the gray levels in the reference state and in the deformed state. Being that the equality is not perfect due to, in the presence of variations of the connected signals, the determination of the shift U requires the minimization of the determination of the optimal values of the transformation parameters is given by the minimum of the quantity $C=\sum_{x\in D} (f(x)-g(\phi(x)))^2$ called "the coefficient of correlation". The displacements are defined by a plane material transformation linking the coordinates of the reference state to the one of deformed state by the following equation:

$$x = \varphi(x) \tag{1}$$

2.2.1 Mark tracking method

The Mark tracking method offers a straightforward optical approach for discerning displacement and strain fields. Following the method's principle, multiple black marks are strategically positioned on the surface of the sample for experimental measurements. A CCD camera, positioned perpendicular to the surface, captures digital images of these markers in each configuration of the sample.
The essence of the method lies in the subsequent tracking of these markers during the test, achieved by computing their geometric centres as reflected by the Gray levels in the images. Notably, the Mark tracking technique exhibits a comparable level of accuracy to the DIC method, establishing it as a reliable alternative for precise measurements in the realm of displacement and strain field analysis [8].

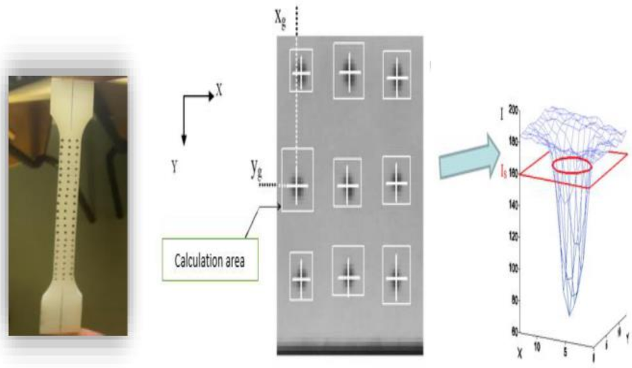

Figure 5 Mark tracking method [8].

ISSN 1590-8844
International Journal of Mechanics and Control, Vol. 25, No. 01, 2024

2.2.2 Assessment of uncertainty from displacement tests

For each imposed translation, the GAP between imposed and measured displacement for the i-th subset is determined according to the translation direction:

$$\Delta u_{i,j} = u_{i,j}^{measured} - u_{i,j}^{imposed} \tag{2}$$

where $u_{i,j}^{measured}$ is the evaluation of the displacement field.
The GAP average is calculated between GAP value and the position of each displacement [9].
The standard deviation σ_u is calculated for each pair of images, by [10]:

$$\sigma_u = \sqrt{\frac{n \sum_{i,j} \Delta u_{ij}^2 - \left[\sum_{i,j} \Delta u_{ij}\right]^2}{n(n-1)}} \tag{3}$$

where n is the number of positions (i, j) for which the displacement is evaluated, whereas the arithmetic mean is obtained as:

$$\overline{\Delta u} = \frac{\sum_{i,j} \Delta u_{ij}}{n} \tag{4}$$

3 RESULTS AND DISCUSSION

3.1 DIGITAL IMAGE CORRELATION (DIC) RESULTS

To perform the experiments and to make the measurements we used both methods the Digital Image Correlation (DIC) method and the mark tracking method. Initially, measurements were conducted on an A4 printed mark. A CCD camera captured numerical images, recording displacements of the material, specifically 2D measurements on a printed A4 sheet in our case. Approximately 10 displacements, each with a value of 10 micrometres, were performed for each test.
The software developed by the Pprime Institute facilitated the storage of numerical images for each configuration. Subsequently, CORRELA and Deftac calculations were executed for each set of images. Additionally, 2D and 3D measurements of materials were conducted using THz images. The correlation subgroup size was selected to be equal to d = 32 pixels.
The image labelled 'Reference Image' is taken before the deformation load and the other image labelled 'Deformed Image' is taken after the deformation load as shown in Figure 6. After taking the spot photo, the analysis of the digital image correlation is done through the surface deformation parameters, within a selected subgroup size. This is a non-contact experimental technique for moving the surface in the plane. The image is initially captured by a classical camera, in its original position, and the next image is captured after moving 10 micrometres. A speckle pattern is randomly sprayed on a flat white surface. Several attempts were made to obtain an evenly distributed pattern of black paint drops.

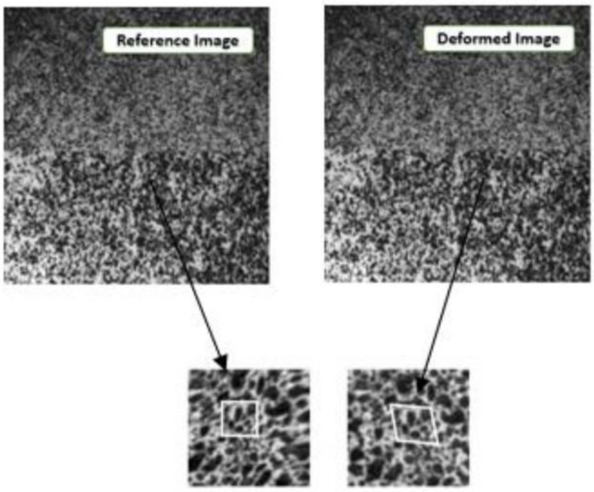

Figure 6 Speckle patterns measurements.

The results obtained from CORRELA software are shown in Figure 7.

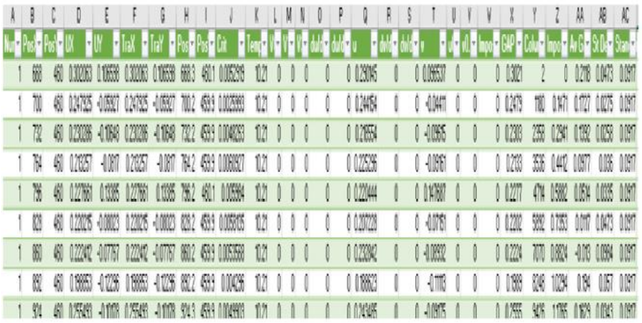

Nur	PosX	PosY	UX	UY	TraX	TraY	Pos	Pos	Crit	Temp	V	V	V	du/dx	du/dy	u	dv/dx	dv/dy	v	u0	v0	Impo	GAP	Colu	Impo	Av G	St De	Stan
1	668	460	0.302063	0.106598	0.302063	0.106598	668.3	460.1	0.005299	10.21	0	0	0	0	0	0.29045	0	0	0.096537	0	0	0	0.3021	2	0	0.2718	0.0473	0.0917
1	700	460	0.247925	-0.05927	0.247925	-0.05927	700.2	459.9	0.0025999	10.21	0	0	0	0	0	0.24454	0	0	-0.0441	0	0	0	0.2479	1180	0.1471	0.1727	0.0275	0.0917
1	732	460	0.230286	-0.10648	0.230286	-0.10648	732.2	459.9	0.0048263	10.21	0	0	0	0	0	0.21654	0	0	-0.0965	0	0	0	0.2303	2358	0.2941	0.1392	0.0258	0.0917
1	764	460	0.213257	-0.0817	0.213257	-0.0817	764.2	459.9	0.0068927	10.21	0	0	0	0	0	0.22526	0	0	-0.0961	0	0	0	0.2133	3536	0.4412	0.0977	0.036	0.0917
1	796	460	0.227661	0.13385	0.227661	0.13385	796.2	460.1	0.005994	10.21	0	0	0	0	0	0.22044	0	0	0.14687	0	0	0	0.2277	4714	0.5882	0.0514	0.0335	0.0917
1	828	460	0.220215	-0.08023	0.220215	-0.08023	828.2	459.9	0.0058105	10.21	0	0	0	0	0	0.20728	0	0	-0.0715	0	0	0	0.2202	5892	0.7353	0.0117	0.0473	0.0917
1	860	460	0.22412	-0.07767	0.22412	-0.07767	860.2	459.9	0.0053568	10.21	0	0	0	0	0	0.23842	0	0	-0.0832	0	0	0	0.2224	7070	0.8824	-0.013	0.0984	0.0917
1	892	460	0.198653	-0.1236	0.198653	-0.1236	892.2	459.9	0.004256	10.21	0	0	0	0	0	0.18623	0	0	-0.1113	0	0	0	0.1989	8248	1.0294	0.184	0.057	0.0917
1	924	460	0.255493	-0.1008	0.255493	-0.1008	924.3	459.9	0.0049903	10.21	0	0	0	0	0	0.24345	0	0	-0.0975	0	0	0	0.2555	9426	1.1765	0.1629	0.0343	0.0917

Figure 7 Results obtained from CORRELA software.

The standard deviation and the imposed displacement were calculated for each pair of images as shown in Figure 8.

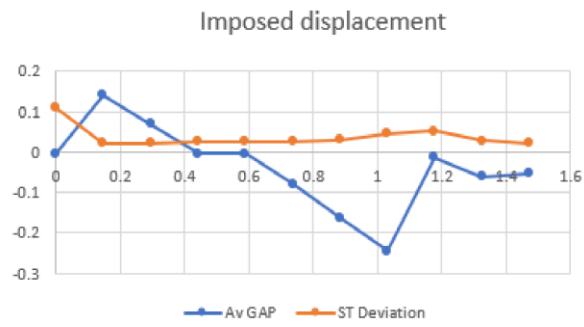

Figure 8 Displacement error versus imposed displacement

From the experimental results, we can see that the standard deviation decreased along with the larger subgroup size, while the mean value remained almost constant. The standard deviation is equal to eight grey levels.

For the main bias, the curve becomes a triangular shape, and the maxima (0,15 pixels), are enlarged and move closer to the integer values of displacement. The value of standard deviation increases to 0.05 and varies little expect for integer values of displacement where the standard deviation is maximum equal to 0,12. Other measurements were performed with different subsite sizes, including d = 8pixels, d = 16pixels, d = 32 pixels, and d = 64 pixels to see the results of the standard deviation error versus the number of pixels of the DIC subsets as shown in Figure 9.

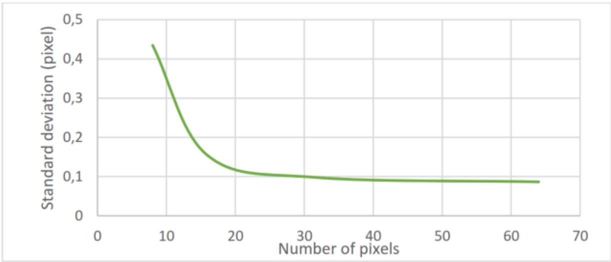

Figure 9 Standard deviation error versus number of pixels of DIC subset for the reference speckle pattern.

The standard deviation errors of the u-displacement for test image pairs with subset sizes ranging from 8x8 pixels to 64 ×64 pixels. It is obvious that, for all three test image pairs, the SD errors decrease as the subset size increases.

Figure 10 presents the evolution of the random error function of the prescribed displacement τ for various image noises, obtained for the standard speckle size (r = r0) and the reference subset size d = 32 pixels. To find uncertainty, three main elements are included, such as subset, image noise, and gradient level. For this reason, it is calculated the Gradient Level (GL).

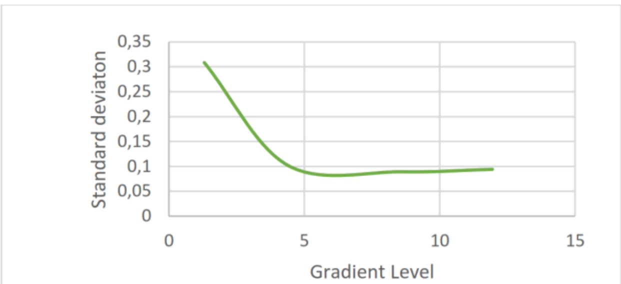

Figure 10 Standard deviation error versus subset size (pixel).

The relationship between the mean displacement error (Δu^c), the standard deviation of the displacement error ($\sigma^c u$), the standard deviation of the image noise (σ_n), and the mean squared Gray level gradients (∇I^2) and the subset size d is given by the following equation:

$$\begin{Bmatrix} \overline{\Delta u}^2 = 0 \\ \sigma_u^c \propto \dfrac{\sigma_n}{d\sqrt{\nabla I^2}} \end{Bmatrix} \quad (5)$$

3.2 MARK TRACKING METHOD RESULTS

The marks tracking method allows to define limits of the study zone. The black marks are positioned manually on the specimen surface. Moreover, to have a good contrast the black marks are positioned on the white background painted on the specimen surface. The Mark tracking method was performed by using Deftac software developed by PEM team of Pprime Institut of Poitiers. Five combinations of marks were considered (different diameters), as shown in Figure 11 the displacements of each mark were measured.

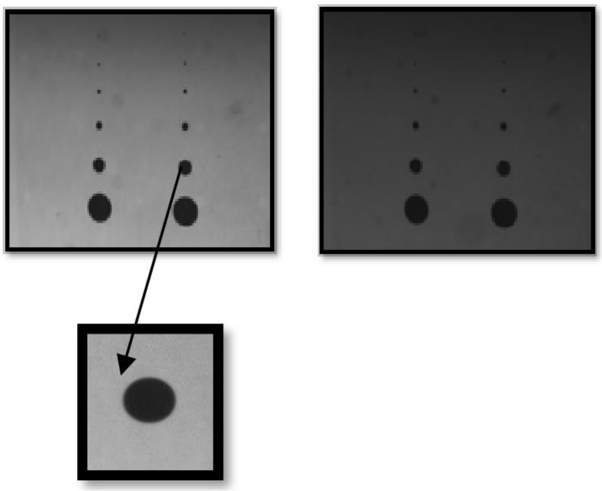

Figure 11 Speckle patterns in mark tracking method.

The results of the measurements for each specimen are shown in Figure 12 and 13

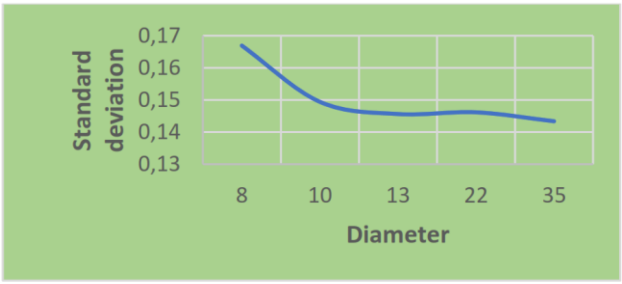

Figure 12 Standard deviation vs Diameter.

Figure 12 shows the evolution of the error of the standard deviation to the diameter of the marks. The graph shows all the diameters of the markers. From the graph, we see that we have a decrease in the error of the standard deviation with the increase of the diameter. In Figure 13, the evolution of the error of the standard deviation against the image contrast is plotted. Images with different contrasts were taken, and we see that the SD error decreases with the increase of contrast (better image contrast). Since we still did not know the contrast of the images that would be obtained through Terahertz waves, it would be interesting to see the contrast variation.

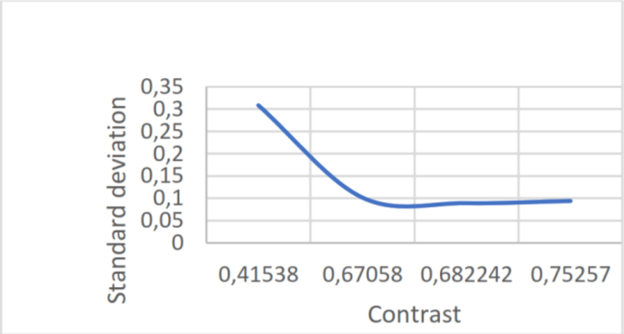

Figure 13 Standard deviation vs Contrast.

3.3 TERAHERTZ WAVE RESULTS

The images of the specimens for fiberglass composite materials are shown in Figure 14 and are realized through Terahertz waves. The size of the correlation subset is chosen equal to d = 32 pixels. The acquisition is realized by scanning a measurement point, one line after the other. The acquisition was carried out in about 10 min on the laboratory bench. The magnification of images is equal to 1 (=1).

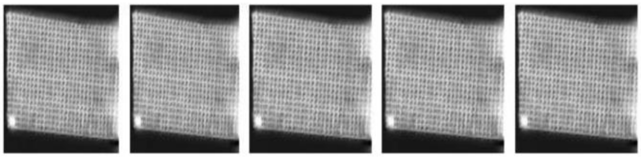

Figure 14 Fiberglass composite images with Terahertz waves.

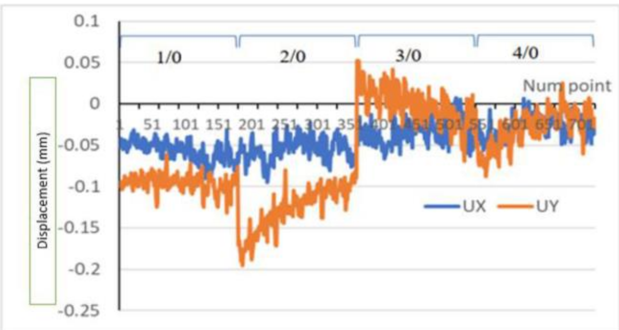

Figure 15 Displacements measured for a correlation window dimension of 32 pixels.

Image displacement measurements were performed through DIC. The size of the subgroup in our case is 32 x 32 pixels. The measurement results of both Ux and Uy axes are given in Figure 15. Through this graph is given the evolution of displacements for 4 measurements (series) performed, in the first case (0-1) we see that we have a displacement for about (-0.05) pixel along to X axis and a displacement for about (-0.1) pixel along to Y axis. In the second step (1-2) we observe a variation of the displacement along y direction. The displacement is larger in the Uy axis due to the rotation of the specimen in this direction.

A variation in displacements Uy is observed. The distribution of displacements is represented in Figure 16. It is observed that this variation evolves between the bottom and the top of the image. We can consider a rotation of the part (along the x-axis of the order of 0.015°) but in this case, we would also have deviations along x which is not the case. For the 3rd state, there is a return to the initial position with again a variation in displacements next y.

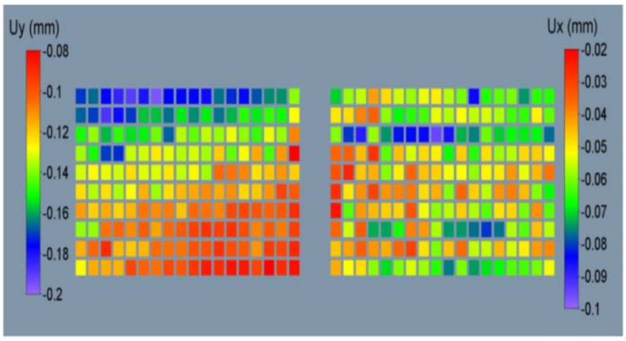

Figure 16 Measured displacements, condition 2/0.

According to [11] the deformations make it possible to confirm that the first condition is a global movement along the xy plane because the deformations are almost zero (standard deviation of 10-4). Then, for state 2, the displacement gradient results in a positive strain Eyy of 7 10-4 in the upper part of the figure and 2 10-4 in the lower part. Along the horizontal the deformations Exx are constant as shown in Figure 17.

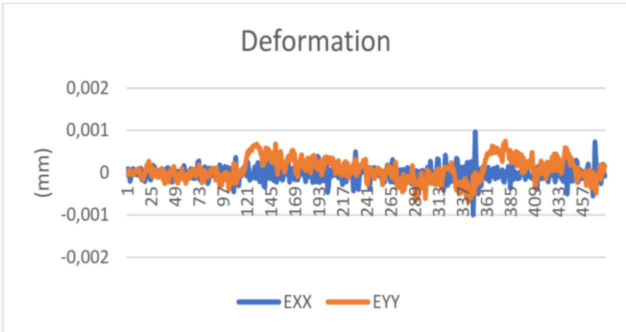

Figure 17 Measured deformation for a correlation window dimension of 32 pixels and a spacing of 64 pixels.

On the x-axis we have constant deformation, in the second state, we have deformation (positive) in the y-axis, up to the value 0.00061 mm, in the third state constant deformation with a small negative fluctuation. And in the fourth state again positive deformation in the y-axis, up to the value of approximately 0.00074 mm.

There are two types of parasitic displacements, a general displacement that can be due to a movement of the part or the acquisition system, and a variable displacement along the image vertical [12]. These differences can be explained by the acquisition method.

For point-by-point image acquisition, these deviations can be due to changes in the scanning step. The images of the specimens for CHC fiberglass (non-composite) materials are shown in Figure 18 and are realized through Terahertz waves.

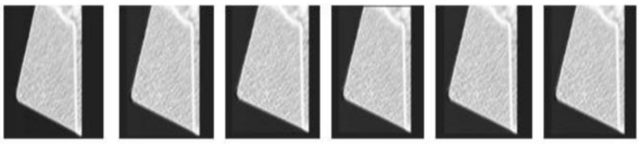

Figure 18 CHC fiberglass (non-composite) images with Terahertz waves.

Six images were taken, which makes five displacement fields measured concerning the first frame (0). In Figure 18 it is observed a very significant fluctuation of the overall displacements of the order of 0.8mm along x a little less along y. This is because the first image was not taken on the same day as the subsequent ones. It is therefore slightly different, which does not allow a precise correlation. On the other hand, by taking image 2 as the reference image and switching the first image last, we obtain much less noisy results We find the same trends as in the previous test with a displacement following y always variable along the vertical of the image. These variations can again be explained by scanning errors.

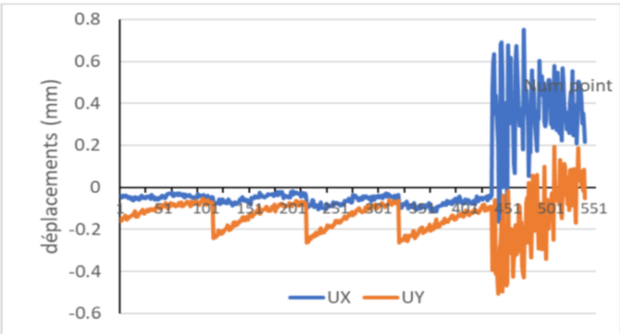

Figure 19 Displacements measured for a correlation window dimension of 32 pixels.

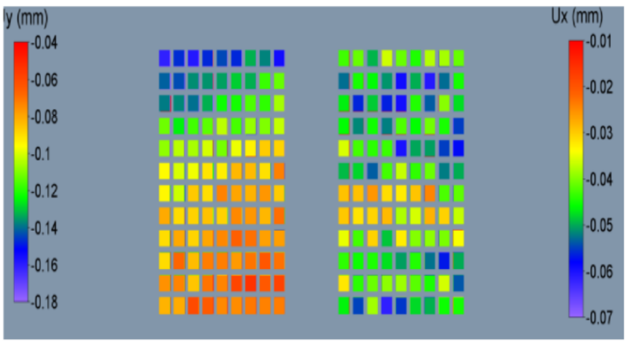

Figure 20 Field of displacements measured in the 1st state for a window size of correlation of 32 pixels.

On the other hand, we find these errors in the 4 states with an overall movement of 0.2 mm. The measurement results of both Ux and Uy axes are given in Figures 19 and 20. We find the same trends for Eyy in Figure 21 as in the first case, the distribution is on the other hand more stepped with two distinct zones [13]. Along the horizontal the deformations Exx are constant. The standard deviation of Exx is slightly smaller than in the 1st case: 8 10-5. This confirms the fact that the quality of the images is good in terms of contrast for the image correlation.

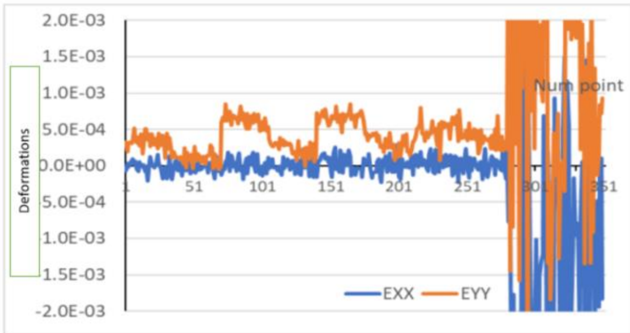

Figure 21 Deformations measured for a correlation window dimension of 32 pixels and a pitch of 64 pixels.

The same conclusions are derived as for the first case. The main error comes only from the scanning technique.
The images of the specimens for white structure with holes materials are shown in Figure 22 and are realized through Terahertz waves.

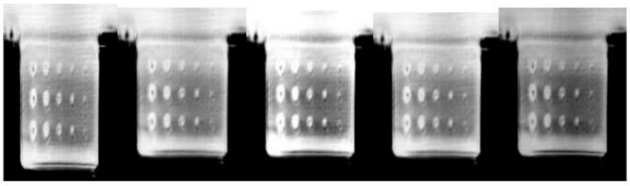

Figure 22 White structure with holes images with Terahertz waves.

Five images were acquired, making four displacement fields measured relative to the image first (0). Generally, we see that we have a constant displacement along x (horizontal) at a maximum value of 0.25 in the upper part of the figure and 0.37 in the lower part. For the first condition (between image 1 and 0) we observe in Figure 23 an overall displacement of 0.4 mm along y (vertical) The same displacement line is maintained in the other three states measured for a correlation window dimension of 32 pixels.
The results are not clear due to the propagation of electromagnetic waves on the material. In this case, the phenomenon of refraction occurs. The purpose and perspective are to take images in materials that consist of holes in a square shape and not circular.

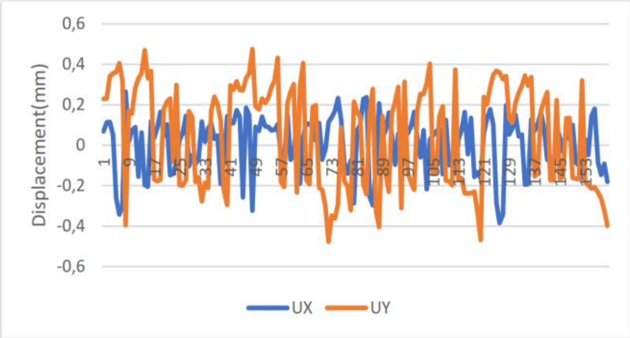

Figure 23 Displacements measured for a correlation window dimension of 32 pixels.

4 CONCLUSIONS

Designing a machine capable of testing various materials and structures for form and composition, as well as assessing compression, traction, and flexibility, presents a significant and challenging undertaking. The complexity arises from the need to integrate these diverse testing functions into a single machine, considering additional factors such as space constraints in the work environment and the requirements for installation within the acquisition system utilizing terahertz waves. In our research, we explored two optical methods suitable for Terahertz image analysis to evaluate their performance in terms of accuracy, contrasts, gradients, and mark size. During the initial analysis of Terahertz images, we identified that the primary source of error stems from the scanning of the sample. This finding indicates the feasibility of measurements and suggests that an initial study could focus on assessing the device, with the potential for enhancing the setup. The primary objective of our study was to precisely assess the capabilities of Terahertz imaging in characterizing the stresses and deformations induced in materials during loading. The obtained results indicate that it is indeed possible to test materials internally using terahertz waves. In conclusion, our work highlights the potential of Terahertz imaging for evaluating material performance under stress, emphasizing the feasibility of internal material testing through terahertz waves.

REFERENCES

[1] T.S. Hartwick, D.T. Hodges, D.H. Barker and F.B. Foote, Far infrared imagery. *Applied Optics 15*, pp. 1919-1922, 1976.

[2] B.B. Hu and M.C. Nuss, Imaging with terahertz waves. *Optics Letters*, Vol. 20, No. 16, pp. 1716-1718, 1995.

[3] W.L. Chan, J. Deibel and D.M. Mittleman, Imaging with terahertz radiation. *Reports on Progress in Physics*, Vol. 70, No. 8, 2007.

[4] P.U. Jepsen, D.G. Cooke and M. Koch, Terahertz spectroscopy and imaging – Modern techniques and applications. *Laser & Photonics Review*, Vol. 5, No. 1, pp. 124-166, 2011.

[5] D.M. Mittleman, Twenty years of terahertz imaging. *Optics Express*, Vol. 26, No. 8, pp. 9417-9431, 2018.

[6] I. Hosako and N. Oda, Midas-KentechTHz Technology https://midas.kentech.ac.kr/page.php?p_id=research1, 2011. [Accessed 10 February 2024].

[7] M. Quanjin, M. Rejab, Q. Halim, M. Merzuki and M. Darus, Experimental investigation of the tensile test using digital image correlation (DIC) method. *Materials Today*, Vol. 27, No. 2, pp. 757-763, 2020.

[8] Y. Barranger, P. Doumalin, J.C. Dupré and A. Germaneau, Strain Measurement by Digital Image Correlation: Influence of Two Types of Speckle Patterns Made from Rigid or Deformable Marks. *Strain*, Vol. 48, 2012.

[9] Y. Belrhiti, A. Gallet-Doncieux, A. Germaneau, P. Doumalin, J.C. Dupre, A. Alzina, P. Michaud, I. Pop, M. Huger and T. Chotard, Application of optical methods to investigate the non-linear asymmetric behavior of ceramics exhibiting large strain to rupture by four-points bending test. *Journal of the European Ceramic Society*, Vol. 32, No. 16, pp. 4073-4081, 2012.

[10] J. Dupre, P. Doumalin, H.A. Husseini, A. Germaneau and F. Brémand, Displacement Discontinuity or Complex Shape of Sample: Assessment of Accuracy and Adaptation of Local DIC Approach. *Strain*, Vol. 51, No. 5, pp. 391-404, 2015.

[11] Alimhillaj P., Pocari S., Lamani, L. and Dorri A., Numerical model and simulation for the influence of temperature on the pressure control valve in an oleodynamic system. *International Journal of Mechanics and Control*, Vol. 24, No. 2, pp. 63-68, 2023.

[12] Cosenza C., Malfi P., Nicolella A., NiolaV., Savino S. and Spirto M., Experimental approach to study the tribological state of gearwheel through vision devices. *International Journal of Mechanics and Control*, Vol. 24, No. 1, pp. 61-68, 2023.

[13] Dell'Osa A.H., Mailing A., Flaherty E., Concu A. and Felice C., Non-invasive in-situ rapid detection of human ankles fractures using the cole model and machine learning. *International Journal of Mechanics and Control*, Vol. 24, No. 1, pp. 197-206, 2023.